Tissue Engineering/Biomaterials

OPEN

Fabrication of Porous Hydroxyapatite Scaffolds as Artificial Bone Preform and its Biocompatibility Evaluation

Dong-Woo Jang,* Rose Ann Franco,* Swapan Kumar Sarkar,* and Byong-Taek Lee*

In this study, a novel porous hydroxyapatite scaffold was designed and fabricated to imitate natural bone through a multipass extrusion process. The conceptual design manifested unidirectional microchannels at the exterior part of the scaffold to facilitate rapid biomineralization and a central canal that houses the bone marrow. External and internal fissures were minimized during microwave sintering at 1,100°C. No deformation was noted, and a mechanically stable scaffold was fabricated. Detailed microstructure of the fabricated artificial bone was examined by scanning electron microscope and X-ray diffractometer, and material properties like compressive strength were evaluated. The initial biocompatibility was examined by the cell proliferation of MG-63 osteoblast-like cells using MTT (3-(4,5-dimethylthiazol-2-yl)-2,5-diphenyltetrazolium bromide) assay. Preliminary *in vivo* investigation in a rabbit model after 4 weeks and 8 weeks of implantation showed full osteointegration of the scaffold with the native tissue, and formation of bone tissue within the pore network, as examined by microcomputed tomography analyses and histological staining. Osteon-like bone microarchitecture was observed along the unidirectional channel with microblood vessels. These confirm a biomimetic regeneration model in the implanted bone scaffold, which can be used as an artificial alternative for damaged bone. *ASAIO Journal* 2014; 60:216–223.

Key Words: bioceramics, extrusion, microstructure, calcium phosphate, layered ceramics

Human cortical bone is a naturally occurring composite material where around two thirds is composed of hydroxyapatite (HAp) nanocrystal.[1] The distinctive characteristics of hard tissues in natural bone are the haversian lamellae, composed of columnar osteons, which are distributed into a concentric circle shape randomly around a central cavity containing bone marrow. Because of this complex microstructure, producing artificial bone similar to natural bone structure is quite challenging. For successful fabrication of artificial bone, the internal architecture of the bone should ensure microarchitecture formation by guiding the natural regeneration process. Several reviews have been published on the general properties and design features of biodegradable and bioresorbable polymers and scaffolds for artificial bone fabrication.[2–4]

Bone is constantly undergoing remodeling processes. Critical-sized bone defects, which are inherently very difficult to heal by the bone remodeling process, need artificial aid to help the remodeling process cover up the defect site relatively shortly and with ease. The treatment has been addressed by autograft, allograft, xenograft, or synthetic bone graft. The former three have limitations in use due to problems of availability, collateral site damage, morbidity, disease transmission, or rejection by the body. Synthetic materials are a common option for bone defect repair.

Studies have demonstrated that a porous microstructure is essential for fast osteointegration and proper bone cell ingrowth in artificial bone grafting. Therefore, scaffolds for bone tissue engineering must have porous structure with consideration of the size, shape, connectivity, and porosity of the pores.[5,6] Accordingly, the design of porous implant materials with pore size larger than 150 μm appears to be suitable size for clinical bone graft applications. The design of porous implant materials with microstructure that mimics the bimodal structural configuration of bone (cortical and cancellous) and with a sufficient degree of interconnectivity[5] is a unique challenge.

Porous structures have inherently poor mechanical properties. Thus, a key problem in artificial bone fabrication is how to construct an osteoinducive microarchitecture with proper connectivity and biological performance without too much neglecting the mechanical strength. The conventional techniques for scaffold fabrication include fiber bonding, solvent casting, particulate leaching, membrane lamination, melt molding, polymer foaming, solid–liquid phase separation, textile technologies, and electrospinning.[7–10] However, with traditional processing methods, the bionic microarchitecture could not be ensured. The logical choices of materials for artificial bone are HAp or tricalcium phosphate ceramic materials or a mixture of the two. These materials not only support favorable cell–material interaction but also promote bone ingrowth *in vivo* (osteoconduction).[11,12]

Bone remodeling is a multicellular phenomenon, which produces osteon bone mineral and also permits repair of microdamage.[13] The distinctive characteristics of hard tissues in natural bone are the haversian lamellae, which are composed of columnar osteons, with the osteons distributed and connected into a concentric circle shape around a central axis. Because of this, it has been considered that producing artificial

From the *Department of Biomedical Engineering and Materials, College of Medicine, Soonchunhyang University, Cheonan, Korea.

Submitted for consideration May 2013; accepted for publication in revised form November 2013.

Disclosure: The authors have no conflicts of interest to report.

This work was supported by the Mid-career Researcher Program through the NRF grant funded by the MEST (No. 2009-0092808).

Reprint Requests: Byong-Taek Lee, Department of Biomedical Engineering and Materials, College of Medicine, Soonchunhyang University, Cheonan 330–930, Korea. Email: lbt@sch.ac.kr.

DOI: 10.1097/MAT.0000000000000032

bone similar to natural bone is quite difficult due to the complex microstructure of natural bone. For a successful fabrication of natural bone, the internal architecture of the bone should be such that the scaffold not only ensures the formation of the characteristic microarchitecture but also guides the natural regeneration process for natural-bone-like organization.

Current research mainly involves the fabrication and improvement of critical-sized defect sites by block, granular, or injectable bone substitutes. But replacing a whole bone section or using artificial bone within load-bearing region is basically different thing. Providing hierarchical architecture and at the same time ensuring the functional organization of different parts of the bone is a challenging task that needs a holistic approach for a successful design.

Many have tried to fabricate microstructures that mimic human bone and contain many micropores using HAp/collagen composites.[14] Porous HAp was investigated as artificial bone application[15] but obtaining complex geometry of natural bone was not assured. New methods with stem cell approach are being investigated to fabricate artificial bone, but the robustness of the bone and the load-bearing ability of it are yet to achieve. A combination of sponge replica and electrospinning method addressed the unidirectional structure and cortical trabecular combined approach, but this too was devoid of significant load-bearing ability and scope for further improvement.[9] We have already developed methods to prepare unidirectional, mechanically stable porous bodies with pore size suitable for bone regeneration.[16] But mismatch of the thermal expansion coefficient of ZrO_2 with that of HAp led to extensive cracking. Although our second attempt[17] successfully controlled the structural integrity in the sintered scaffold, the presence of a bioinert phase prohibited the full biointegration. In the current study, we tried to fabricate all HAp porous bone preform that could be used to guide a biomimetic regeneration process after implantation. Detailed analysis of the microstructure and materials properties was conducted. In addition, the biocompatibility of the artificial bone with porous microstructure was investigated using *in vitro* and *in vivo* experiments.

Experimental Procedure

Extrusion Process for Fabricating Porous Composites

An HAp nanopowder was synthesized in-house by precipitation method. Ethylene vinyl acetate copolymer (ELVAX 210A; Dupont, Wilmington, DE), carbon powder (<15 μm, Aldrich, St. Louis, MO), and stearic acid (Daejung Chemicals & Metals Co., Korea) were used as a thermoplastic binder, pore forming agent, and lubricant, respectively. A shear-mixed green composite (50 vol %/HAp 40 vol %/polymer 10 vol %/stearic acid) was prepared with the above materials. HAp shell with 20 mm external diameter and 2 mm thickness was warm pressed in a cylindrical die at 100°C. Shear-mixed carbon (50 vol %/carbon powder 40 vol %/polymer 10 vol %/stearic acid) was prepared using the same process.

Cylindrical carbon core was wrapped by HAp shell to make the feed roll and extruded to make the first filament (3.5 mm in external diameter). A second filament (16 mm in external diameter) was fabricated using the feed roll. The 28 first filaments arranged in the cylindrical die were extruded to make a third filament (3.5 mm in external diameter). The second filament was used as a central axis and wrapped with the 28 third filaments in the die and extruded to make a fourth filament (16 mm in diameter). The fourth filament (16 mm in diameter) was wrapped with a HAp shell and extruded to make the final green preform. Binder was burnt-out at a temperature of 700°C in a flowing nitrogen atmosphere, reaching the final temperature after 7 days. The carbon was burnt-out at 1,000°C at 2°C/minute increment in an air atmosphere through a second burnout process. Finally, microwave sintering of the artificial bone to combine the composites was carried out in air at 1,100°C.

Characterization

The morphologies of the porous HAp composites were observed by scanning electron microscopy (SEM, JSM-7401F) and energy-dispersive spectrometry (EDS, JSM-7401F). The crystal structure of the composite was determined by X-ray diffraction (Miniflex II, Rigaku, Japan). The compressive strength of the samples was measured using a universal testing machine (R&B, Korea).

Compressive Strength Measurement

The cylindrical shape samples were subjected to compressive strength measurement in the axial direction. Universal Testing Machine (R&B, Korea) was used with built-in software to measure the compressive strength. Sample height was chosen as 3 mm and average of five measurements was taken.

In Vitro *Biocompatibility Testing*

MG-63 osteoblast-like cells were obtained from the Korean Cell Line Bank and cultured with Dulbecco's modified Eagle medium (Hyclone, Thermoscientific, Pittsburgh, PA) supplemented with 10% fetal bovine serum (Hyclone) and 1% penicillin/streptomycin antibiotics (Sigma, St. Louis, MO). Quantification of cell growth and proliferation was done using MTT (3-(4,5-dimethylthiazol-2-yl)-2,5-diphenyltetrazolium bromide) assay. Ultrasonically cleaned and then autoclaved samples were put inside 24 well plate and seeded with 10,000 cells per well. The scaffolds were incubated for 1, 3, and 5 days. After incubation, the samples were transferred to a new plate (24 wells). A 200 μl MTT solution was added onto the composite, which was then incubated at 37°C for 3.5 hours, after which the MTT solution was discarded. Then, the dimethyl sulfoxide solution was added to dissolve any insoluble formazan crystals on the samples. From the 24 well plate, 150 μl of solution was transferred to a plate with 96 wells. The absorbance was measured at 595 nm using an enzyme-linked immunosorbent assay (ELISA) or microplate reader (Turner Biosystems CE, Promega Corporation, Sunnyvale, CA) for MTT testing.

The osteoblast cells were seeded on tissue culture polystyrene as control samples and on the scaffold at a concentration of 10^4 cells/ml. Samples were kept at 37°C in a humidified air atmosphere with 5% CO_2 for 1, 3, and 5 days. After the specified duration, the media was removed and the entire cell seeded specimens washed with phosphate buffered saline (PBS) solution and fixed in 4% paraformaldehyde for 15 minutes at room temperature. It was then permeabilized in PBS containing 0.25% Triton X-100 for 10 minutes and blocked in 2.5% bovine serum albumin for 30 minutes. Cells were immunostained using fluorescein isothiocyanate–conjugated phalloidin for 2 hours at room temperature. Nuclei were counterstained with 4′,6-diamidino-2-phenylindole. The scaffold were mounted

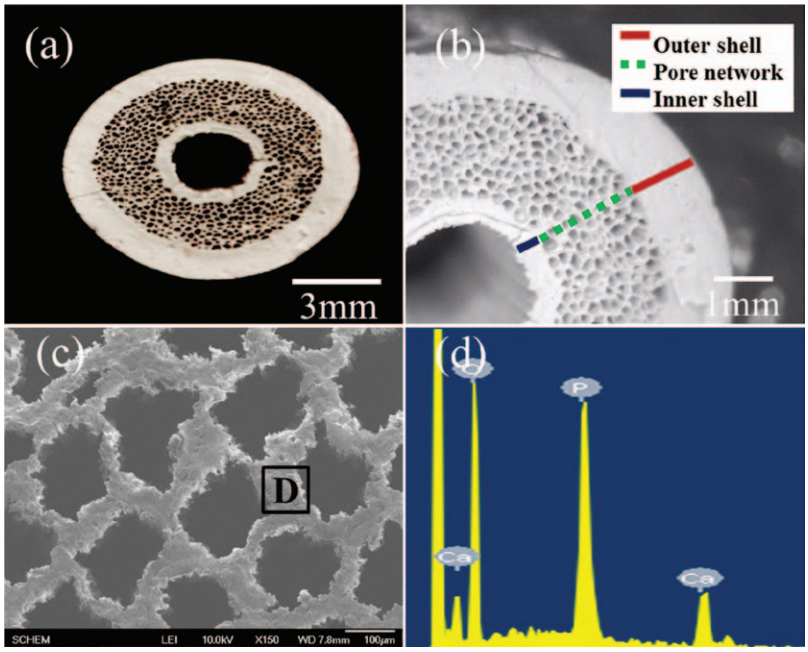

Figure 1. Optical micrograph (**A**), scanning electron micrograph (**B**), detail of the pore network (**C**), and energy-dispersive spectrometry profile (**D**) of hydroxyapatite extruded scaffold after sintering at 1,100°C.

onto glass slides and observed in confocal fluorescent microscope (FV10i-W) using accompanying FV10i-ASW 3.0 software.

In Vivo *Biocompatibility*

Implantation. Implantation of the porous sintered scaffold was done in adult male New Zealand white rabbits each weighing 2.5 kg in average and 2 months old. We used three rabbits for each time span. The scaffold was sterilized by ultrasonic cleaning and then autoclaving. Before animal use with regard to operation, raising and sacrifice approval was obtained from the university ethical committee on animal care and use. The rabbits were raised in animal care unit and were taken care of daily. Urethane was used as anesthesia drug for performing the surgery. After sterilizing the shaved left femur area and sterilizing by Povidon, an incision was made to expose the left femur bone and a circular area was cut with a cylindrical rotary saw with the saw diameter selected to make a cut to fit the sample. The animal was kept in laboratory conditions and fed *ad libitum* and raised for 4 weeks and 8 weeks before sacrifice. Baytiril (enrofloxacin) was used as antibiotic during the postoperation period. No postsurgical pain modification medication was administered. The animals were sacrificed according to university ethical committee guidelines. Before sacrifice, succinylcholine chloride was used to immobilize the rabbit and the femurs were harvested. The harvested bone was fixed in 10% formalin and stored at room temperature before histological analysis.

Micro-CT scanning. A Skyscan Deskop Micro-CT 1172 (Aartselaar, Belgium) with a source voltage of 60 kV and a current of 167 µA was used to acquire X-ray radiographs. After scanning, cross-sectional slices were reconstructed and each scan result was reconstructed using the 0.010–0.067 threshold values to distinguish bone and air.

Histological staining. The section of the formalin-fixed rabbit femur containing the implant's decalcification was carried out by immersing in 5% nitric acid for 2 days and then dehydrating with ethanol series and subsequent xylene immersion for alcohol clearance. Samples were embedded in paraffin wax and cut into 5 µm sections with a microtome (HM 325, Thermoscientific). Tissue sections were deparaffinized and cleared using standard protocol before staining with hematoxylin and eosin (H&E) method and Masson's Trichrome method. Stained sections were viewed with an optical microscope (Olympus BX51, Japan).

Results

Structural Features and Mechanical Properties

The microstructure and design features are shown in **Figure 1A**, in an optical image of the cross section of the sintered scaffold. The outer shell is dense, which gives ideal structural support to the scaffold jointly with the innermost thin shell. The internal pores have very thin walls and are essential

Table 1. Gross Morphological Observation of the Novel Porous Hydroxyapatite Scaffold at Different Sintering Temperatures

Sintering Temperature (°C)	External Fissure	Internal Fissure	Deformation	Postsintering Stability
1,000	(–)	(+)	(–)	(–)
1,100	(–)	(+)	(–)	(+)
1,150	(+)	(+)	(–)	(+)
1,200	(+)	(+)	(+)	(+)
1,250	(+)	(+)	(+)	(+)

Table 2. Dimensional Analyses of Hydroxyapatite Composite Fabricated at 1,100°C and Corresponding Mechanical Strength

Sintering Temperature (°C)	Compressive Strength (MPa)	Internal Diameter (mm)	External Diameter (mm)	Number of pores (ea)	Pore Size (μm)
1,100	3.5 ± 0.28	2.3 ± 0.14	9.4 ± 0.23	784	150 ± 20

for fast resorption of the materials. **Figure 1B** shows the external and internal structure of the optimized HAp scaffold after the polymer binder and graphite were removed, which were measured to have approximately 9.4 ± 0.23 mm outer diameter and 2.3 ± 0.14 mm inner diameter. The size of the pore channel designed to facilitate bone growth was 150 ± 20 μm in diameter. The pore network is shown in detail in **Figure 1C**. The frame of the pores was only 50 ± 10 μm, which is thin enough for very fast osteoresorption. The EDS profile (D) was taken from the D region of the SEM image (C), and it was clearly confirmed that the frame is composed of HAp phase, as evidenced by elevated Ca and P peaks only.

The scaffolds were fabricated at 1,000°C, 1,100°C, 1,150°C, 1,200°C, and 1,250°C. At temperatures higher than 1,100°C, prominent cracks and deformations were seen at the outer thick shell of the scaffold. **Table 1** summarizes the gross morphological observation in the scaffolds. The dimensions and compressive strength of the HAp scaffold were measured five times, and the averages are shown in **Table 2**. The average pore size was 150 ± 20 μm, and the scaffold was designed to have exactly 784 pores within the network by arranging the number of extrusion passes and filament number. The sintering temperature was chosen to be 1,100°C, because higher sintering temperature produced some cracks, and the shape was slightly deformed.

Figure 2 illustrates the XRD profiles of the (A) HAp starting powder and (B) HAp composite sintered at 1,100°C using microwaves. The XRD patterns of the HAp starting powder calcined at 750°C and HAp composite sintered at 1,100°C are shown in **Figure 2, A** and **B**, exhibiting peaks corresponding to the HAp phase. From these results, it can be confirmed that the HAp composite was composed of pure HAp particles.

In Vitro *Biocompatibility*

It was observed that cell growth in the porous sintered scaffold had increased with the lengthening of the culture period,

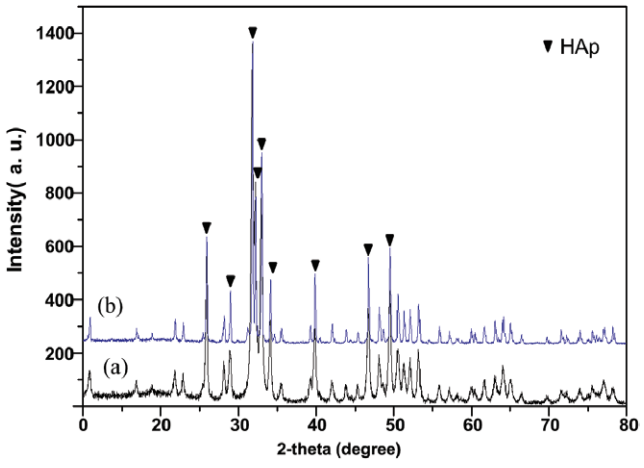

Figure 2. X-ray diffractometer profiles of hydroxyapatite (HAp) starting powder calcined at 750°C (**A**) and HAp composites sintered at 1,100°C (**B**).

which demonstrated the potential of the scaffold to host cell growth and reproduction. Cell density in the scaffolds was comparable to that of the control after 1 and 3 days of culture. Slight increase in the cell density on the porous scaffold over the control was observed on the fifth day (**Figure 3**).

Figure 3, B1 and **C1** shows the gross cell growth on the surface of HAp scaffold after 1 day and 5 days of incubation. It can be observed that cell adherence was prominent on day 1 (**Figure 3B2–B5**). The density of cellular growth increased relatively after 5 days of incubation as cells covered most of the outer shell of the scaffold surface (**Figure 3, C2** and **C3**) as well as the walls of the pore network (**Figure 3, C4** and **C5**).

In Vivo Biocompatibility

Material interaction and bone regenerating ability in a living system were investigated by implanting the scaffold in white New Zealand rabbit model. The scaffold was sterilized and set in drill-cut bone, as shown in **Figure 4A**. Extraction of the femoral grafts was done during the fourth and eighth weeks of implantation. Gross animal appearance appeared to be normal during the entire period of observation.

Micro-CT scanning images were seen in **Figure 5**, showing integration of the sample into the native bone tissue and material degradation after 4 and 8 weeks of implantation. The porous scaffold showed dense, generally intact structure and a clear, brightly colored micro-CT image of the implanted scaffold with natural bone after 4 weeks of grafting (**Figure 5, A1** and **A2**). **Figure 5, B1** and **B2** showed changed color of the implanted scaffold that was similar to natural bone during the eighth week of grafting, which was representative of biodegradation. Bone volume/tissue volume (BV/TV) and bone surface density/tissue volume (BS/TV) measurements of the newly formed bone are shown in **Figure 5**. The BV/TV and BS/TV results show increased values of 57.853 (%) and 2.779 (%) in 8 weeks, compared to 51.627 (%) and 2.05 (%) in 4 weeks, and the changed parameters show that the amount of newly formed bone increased with implantation time.

Histological staining of tissue sections showed implant behavior *in vivo* after 4 weeks and 8 weeks of implantation (**Figure 6, A1** and **B1**, respectively). The bone tissue–scaffold junction during the fourth and eighth weeks showed similar morphological behavior (**Figure 6, A2** and **B2**, respectively). Neat integration of the scaffolds in the native host tissue was observed. No signs of inflammatory cell reaction were noted in the perimeter of the implant. Enlarged details of the scaffold pores showed significant osteoblast cellular activity (**Figure 6, A3** and **B3**). Dense tissue deposition was observed in the pore walls during the eighth week (**Figure 6B3**), which is morphologically similar to the native bone in the bone–scaffold junction. Blood vessel formation was also observed within the pore channel during the fourth week of implantation as a central conduit as indicated by arrow head (**Figure 6, A4** and **B4**). The microblood vessel formation is essential for the increased cellular activity in the deep interior of the

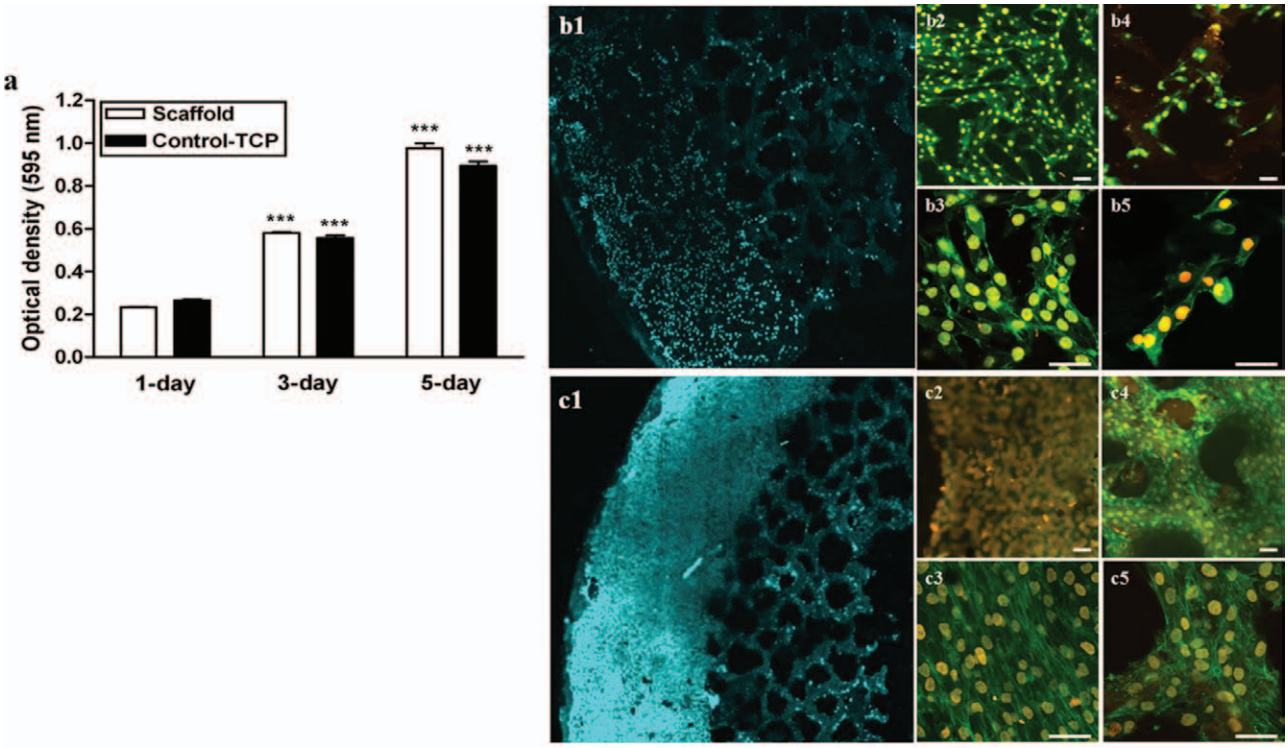

Figure 3. Cell proliferation behavior of MG-63 osteoblast-like cells in the hydroxyapatite scaffold after 1, 3, and 5 days using MTT assay (**A**). Confocal laser micrographs of hydroxyapatite scaffold after 1 day (**B1**) and 5 days (**C1**) of culture with MG-63 osteoblast-like cells. Details of the outer shell section (**B2**, **C2**) and pore network (**B4**, **C4**) were also visualized using higher magnification (**B3**, **C3** and **B5**, **C5**, respectively). Scale bar = 50 μm. TCP, tissue culture polystyrene.

implanted scaffold. This is crucial for the biointegration of the scaffold.

Masson's Trichrome method stains bone and collagen in blue. **Figure 7** shows the bone tissue formation inside the scaffold's pore network during the fourth week and eighth week of implantation (**Figure 7, A1** and **B1**, respectively). Pores located near the center were observed to have dense tissue formation in the pore walls, but structural morphology of the cancellous bone was preserved (**Figure 7B4**). Both H&E staining and Masson's Trichrome staining were duplicated for all the three rabbits, for each time span.

Discussion

Scaffold fabrication for replacing a major part of or an entire organ is a significantly complex task and involves numerous obstacles and challenges. Fabrication of an artificial bone scaffold is not an exception. However, bone mineral phase regenerates its own biological structure periodically and can be used to great advantage for tissue engineering applications. The key is making an optimal design with proper microarchitecture to guide the regeneration process. The porous microstructure achieved by using HAp was designed and studied extensively in artificial aid for bone regeneration and was found to possess osteoconductivity. However, the porosity of a scaffold compromises mechanical properties. In this study, the scaffold was designed to have a porous structure with a narrow range of pore diameters, fabricated by multiextrusion method. This method could easily control the pore size, microstructure, and mechanical strength by changing the extrusion number and pore network layout before extrusion.

In the fabricated scaffold, the porous structure is organized but structurally weak and disintegrates in low load and is not suitable for high load-bearing applications. Very thin pore

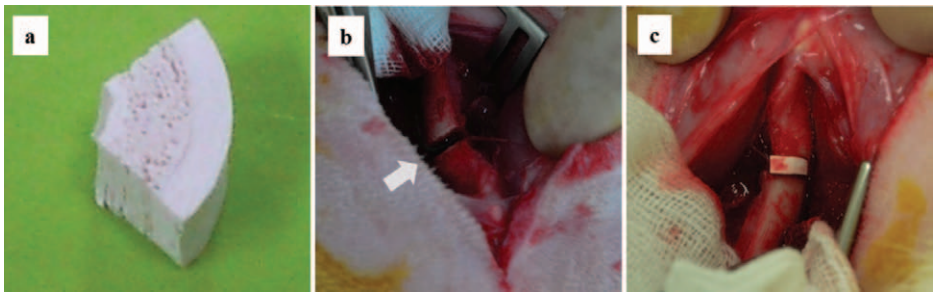

Figure 4. Photomicrographs of novel porous hydroxyapatite scaffold (**A**), defect (arrow) made with the rabbit femur (**B**), and implantation of the hydroxyapatite scaffold on the bone defect (**C**).

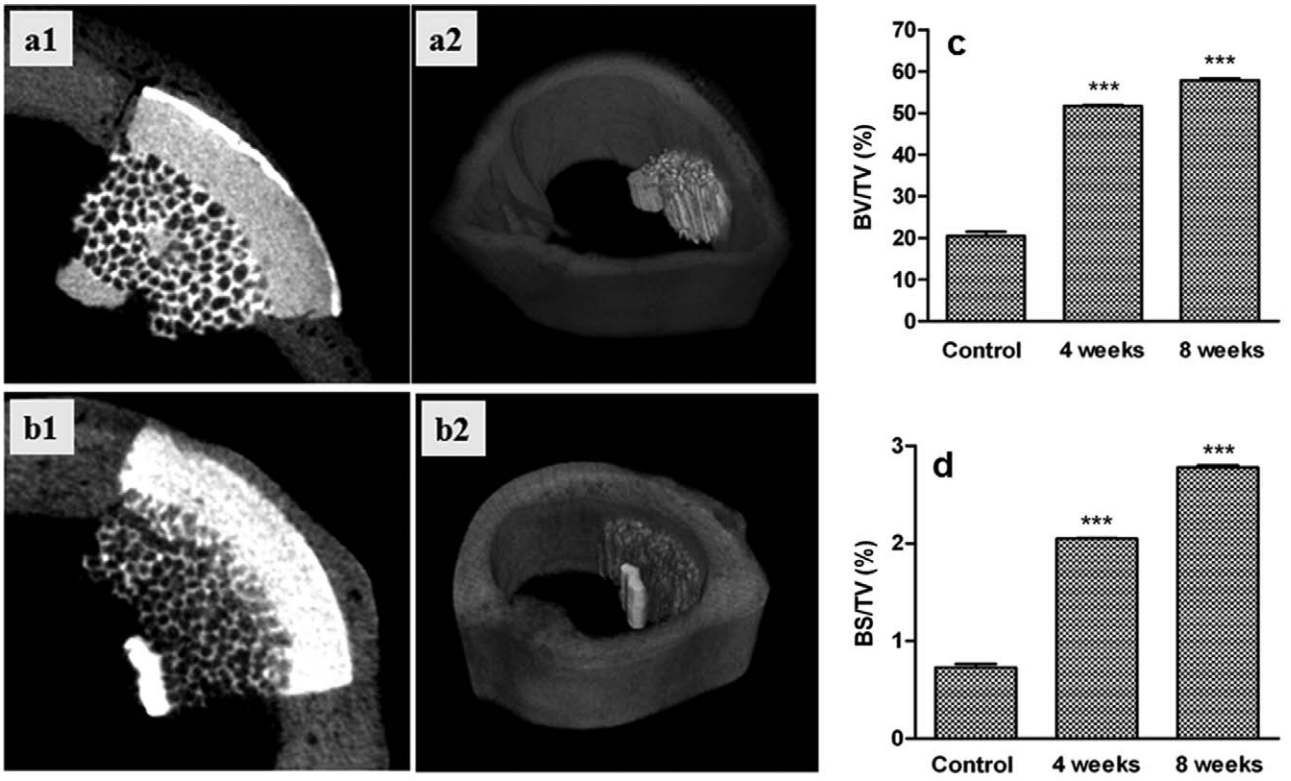

Figure 5. Microcomputed tomography micrographs (**A1** and **B1**) and reconstructed 3D images (**A2** and **B2**) of the porous hydroxyapatite scaffold after 4 weeks (A1 and A2) and 8 weeks (B1 and B2). Percentage bone volume (**C**) and bone surface density (**D**) of implanted scaffold after 4 weeks and 8 weeks of grafting. BS, bone surface density; BV, bone volume; TV, tissue volume.

wall within the porous interior limits the load-bearing ability of the fabricated scaffold, which is reasonable because of the lower strength and fracture toughness of used HAp material. This can be averted by designing a thicker pore wall and higher compressive strength could be achieved, albeit with a compromise of its biodegradation and integration behavior. However, the drawback is partially minimized with the structural support from the strong peripheral thick enclosure. This enclosure at the outer region also ensures the shape of the artificial bone. The proliferative ability and cell adhesion behavior of osteoblast-like cells were investigated. Results showed favorable cell growth pattern and behavior as the cells showed increasing growth rate and nuclear density and increased extracellular material deposition over time. Cells were seen to increase in number as the culture time was lengthened. In connection with the porous network of the fabricated scaffold, porosity produces a biological advantage as it provides a means of nutrient exchange and diffusion

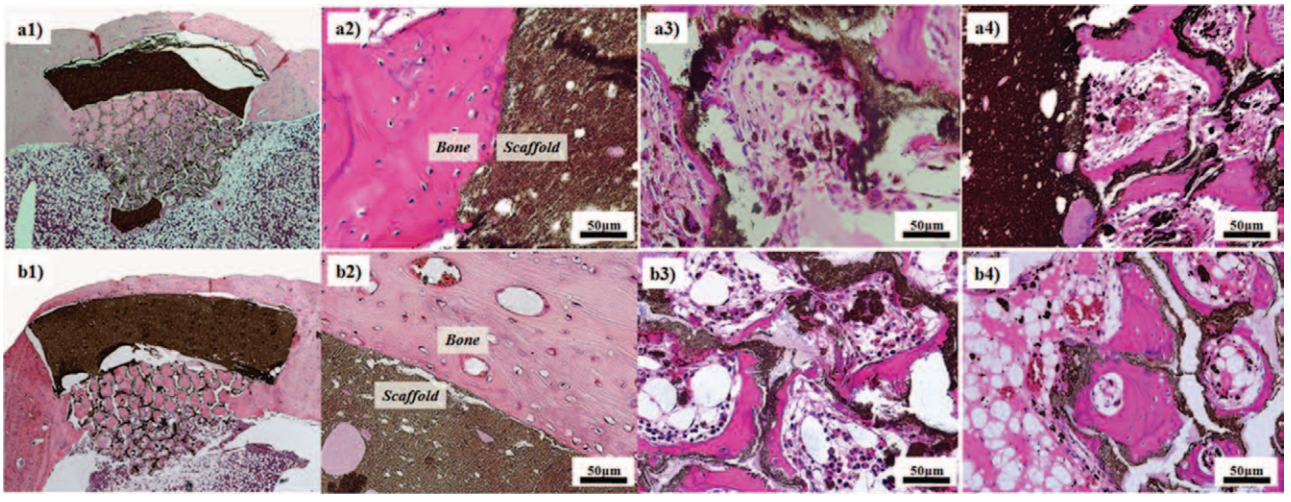

Figure 6. Tissue sections of bone containing the implant during 4 weeks (**A1**) and 8 weeks (**B1**) of implantation. Enlarged micrographs of the bone tissue–scaffold junction (**A2** and **B2**), cellular activity and cell penetration in the pore network (**A3** and **B3**), and possible signs of vascularization (**A4** and **B4**).

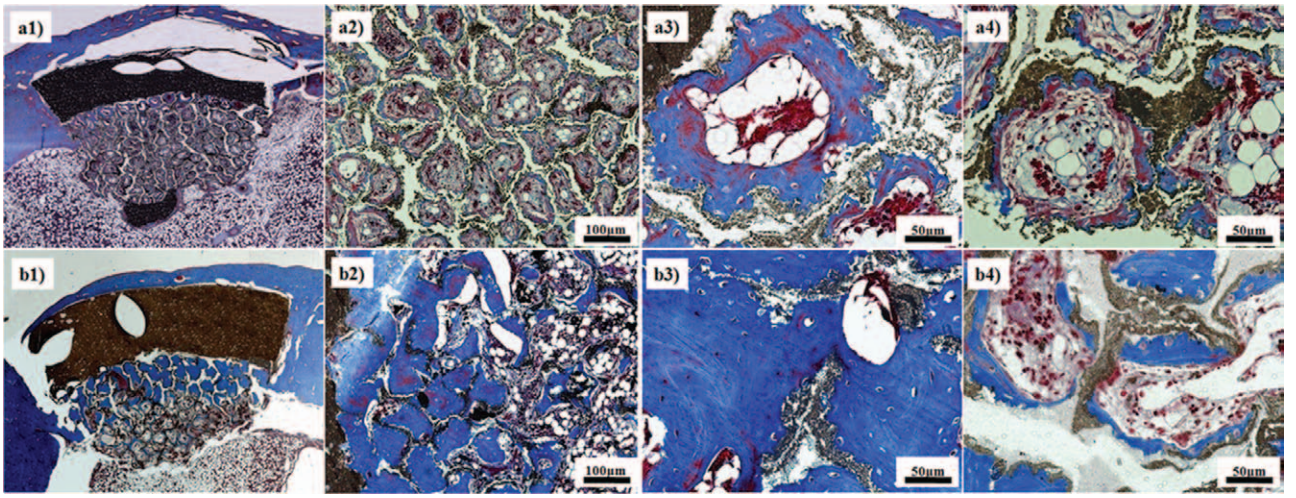

Figure 7. Tissue sections of bone containing the implant during 4 weeks (**A1**) and 8 weeks (**B1**) of implantation. Enlarged micrographs of the pore network (**A2** and **B2**), details of bone tissue formation in the pores near the base of the scaffold (**A3** and **B3**), and pores near the center (**A4** and **B4**).

across the material, thereby providing an optimum environment for cell proliferation. The porous structure has some important features, which allows for cell migration, formation of vascularization, as well as diffusion of nutrients.[18] All the *in vitro* data evidently showed that the expected biocompatibility of the HAp scaffold and microarchitectural features did not pose any hindrance.

The *in vivo* data evidently showed the superior bone regeneration profile using the fabricated scaffold. The results of BV/TV and BS/TV measurements in **Figure 6** reveal the bone formation with the implanted porous artificial bone over time. The newly formed bone filled in the porous microstructure and gradually the whole implanted section was largely ossified.

The interactions between the surfaces of implant and native bone are shown in **Figure 7**. Tissue formation was evident within the pore walls of the scaffold, which appeared denser at a later harvested period. Pores of the scaffold also appeared to be larger at this time, which may have been due to material degradation that took place to accommodate the tissue formation. The dense tissue within the pore was collagen-rich, as detected by Masson's Trichrome staining, and had morphology similar to the native bone.

Histological staining of the sections also showed evidence of vasculature formation (**Figure 7, A4** and **B4**). The supply of nutrients and oxygen necessary for cellular function must be adequate for successful tissue regeneration. The porous design of the inner part of the scaffold allowed both cellular penetration and vasculature. We also analyzed the expression of collagen type I and noncollagenous matrix proteins including osteopontin and osteocalcin. Collagen type I is a matrix protein synthesized by osteoblasts and becomes mineralized with HAp during the latter stages of osteogenesis.

The mentioned biocompatibility indications through the *in vitro* and *in vivo* results provide clear details of the potential of this scaffold for bone tissue regeneration. However, further experimentation is needed to examine the long-term degradation of the HAp scaffold in an animal model, particularly of the dense outer shell, to provide evidence of bone-replacing efficiency. The scaffold can be used as a test bed for further modification for tissue engineering concept by bioactive materials coating and modification and stem cell loading.

Conclusion

Porous HAp scaffold was fabricated as an artificial bone preform using a multipass extrusion process to replace natural bone. The pore size and microstructure of the imitation natural bone were closely related to the extrusion numbers and arrangement of each filament in the last step. The porous structure was sintered without surface cracks at 1,100°C. *In vitro* and *in vivo* tests confirm that the porous microstructure is a relatively good environment for grafting on the scaffold without eliciting inflammatory reaction. Extensive bone formation was evident after 8 weeks of implantation.

References

1. Augat P, Schorlemmer S: The role of cortical bone and its microstructure in bone strength. *Age Ageing* 35-S2: ii27–ii31, 2006.
2. Hutmacher DW: Scaffolds in tissue engineering bone and cartilage. *Biomaterials* 21: 2529–2543, 2000.
3. Hollinger JO, Chaudhari A: Bone regeneration materials for the mandibular and craniofacial complex. *Cells Mater* 2: 143–151, 1992.
4. Hutmacher D, Hürzeler MB, Schliephake H: A review of material properties of biodegradable and bioresorbable polymers and devices for GTR and GBR applications. *Int J Oral Maxillofac Implants* 11: 667–678, 1996.
5. De Oliveira JF, De Aguiar PF, Rossi AM, Soares GA: Effect of process parameters on the characteristics of porous calcium phosphate ceramics for bone tissue scaffolds. *Artif Organs* 27: 406–411, 2003.
6. Lee BT, Kang IC, Cho SH, Song HY: Fabrication of a continuously oriented porous Al_2O_3 body and its in vitro study. *J Am Ceram Soc* 88: 2262, 2005.
7. Lu L, Mikos AG: The importance of new processing techniques in tissue engineering. *MRS Bull* 21: 28–32, 1996.
8. Widmer MS, Mikos AG: Fabrication of biodegradable polymer scaffolds for tissue engineering. in Patrick CW Jr, Mikos AG, McIntire LV (eds), *Frontiers in Tissue Engineering*. New York, Elsevier Science, 1998, pp. 107–120.
9. Kim YH, Lee BT: Novel approach to the fabrication of an artificial small bone using a combination of sponge replica and

electrospinning methods. *Sci Technol Adv Mater* 12: 35002, 2011.
10. van Lenthe GH, Hagenmüller H, Bohner M, Hollister SJ, Meinel L, Müller R: Nondestructive micro-computed tomography for biological imaging and quantification of scaffold-bone interaction in vivo. *Biomaterials* 28: 2479–2490, 2007.
11. Gauthier O, Bouler JM, Aguado E, Pilet P, Daculsi G: Macroporous biphasic calcium phosphate ceramics: Influence of macropore diameter and macroporosity percentage on bone ingrowth. *Biomaterials* 19: 133–139, 1998.
12. Baeza A, Izquierdo-Barba I, Vallet-Regí M: Biotinylation of silicon-doped hydroxyapatite: A new approach to protein fixation for bone tissue regeneration. *Acta Biomater* 6: 743–749, 2010.
13. Burr DB, Forwood MR, Fyhrie DP, Martin RB, Schaffler MB, Turner CH: Bone microdamage and skeletal fragility in osteoporotic and stress fracture. *J Bone Miner Res* 12: 6–15, 1997.
14. Cornell CN, Lane JM, Chapman M, *et al*: Multicenter trial of Collagraft as bone graft substitute. *J Orthop Trauma* 5: 1–8, 1991.
15. Sopyana I, Melb M, Rameshc S, Khalidd KA: Porous hydroxyapatite for artificial bone applications. *Sci Tech Adv Mater* 8: 116–123, 2007.
16. Jang DW, Kim YH, Lee BT: Microstructure control of TCP/TCP-(t-ZrO_2)/t-ZrO_2 composites for artificial cortical bone. *Mater Sci Eng C* 8: 1660–1666, 2011.
17. Jang DW, Nguyen TH, Sarkar SK, Lee BT: Microwave sintering and in vitro study of defect-free stable porous multilayered HAp–ZrO_2 artificial bone scaffold. *Sci Technol Adv Mater* 3: 035009, 2012.
18. Lu JX, Flautre B, Anselme K, Hardouin P, Gallur A, Descamps M: Role of interconnections in porous bioceramics on bone recolonization in vitro and in vivo. *J Mater Sci Mater Med* 10: 111–120, 1999.